Interaction and variability of ice streams under a triple-valued sliding law and non-Newtonian rheology

Roiy Sayag[1] and Eli Tziperman[2]

Received 2 August 2010; revised 14 November 2010; accepted 20 December 2010; published 17 February 2011.

[1] Ice streams are regions of fast flowing glacier ice that transport a significant portion of the total ice flux from present ice sheets. The flow pattern of ice streams can vary both temporally and spatially. In particular, ice streams can become stagnant and change their path. We study the dynamics of ice streams using an idealized model of an isothermal and power law viscous ice flow that includes horizontal (lateral) shear stresses. The basal sliding law is assumed to be triple-valued. We investigate the spatiotemporal patterns formed because of the flow over a flat bed, fed from an upstream mass source. The ice flows from the mass source region through one or two gaps in a prescribed upstream topographic ridge which restricts the flow, leading to the formation of one or two ice streams. We find a relation between the parameters of the ice rheology and the width of the ice stream shear margins and show how these parameters can affect the minimum width of an ice stream. We also find that complex asymmetric spatiotemporal patterns can result from the interaction of two ice streams sharing a common mass source. The rich spatiotemporal variability is found to mostly be a result of the triple-valued sliding law, but non-Newtonian effects are found to play a significant role in setting a more realistic shear margin width and allowing for relevant time scales of the variability.

Citation: Sayag, R., and E. Tziperman (2011), Interaction and variability of ice streams under a triple-valued sliding law and non-Newtonian rheology, *J. Geophys. Res.*, *116*, F01009, doi:10.1029/2010JF001839.

1. Introduction

[2] Ice streams are bands of fast flowing ice embedded within a region of slower ice flow that are observed in the present ice sheets and may have been active in past ice sheets. In Antarctica, ice streams cover merely 10% of the ice sheet surface but may account for about 90% of the ice transport [*Bamber et al.*, 2000; *Bennett*, 2003]. Observational evidence suggests that the pattern of ice stream flow can change both spatially and temporally and that ice streams were possibly involved in events of past ice sheet collapses [*Heinrich*, 1988; *MacAyeal*, 1993a, 1993b; *Marshall and Clarke*, 1997]. Understanding the dynamics of ice streams is therefore important to be able to predict the evolution of ice sheets on many time scales.

[3] The ice streams in the Siple Coast, which drain part of the West Antarctic Ice Sheet, extend over a length of several hundreds of kilometers and are 20–50 km wide. The velocity contrast between the stream and the interstream regions can be two orders of magnitude, which results in high horizontal (lateral) shear stresses at the few kilometers wide ice stream margins [*Echelmeyer et al.*, 1994]. This suggests that horizontal shear stresses may be dynamically important in the vicinity of the shear margins. Observations indicate that shear margins of some ice streams can change their position at an average speed of the order of 100 m/yr [*Bindschadler and Vornberger*, 1998]. Some evidence also suggests that regions that were active streams several hundreds of years ago are currently stagnant [*Retzlaff and Bentley*, 1993; *Jacobel et al.*, 2000; *Catania et al.*, 2006], or being crossed by more recent ice streams [*Gades et al.*, 2000; *Conway et al.*, 2002]. This spatiotemporal behavior may be the consequence of a competition of several ice streams over a common mass source [*Anandakrishnan and Alley*, 1997; *Joughin et al.*, 1999].

[4] The topography beneath the Siple Coast ice streams seems to, at most, weakly constrain the flow of the ice stream trunks. In particular, no consistent relation between the shear margin position and the bottom topography has been identified [*Raymond et al.*, 2001]. This is in contrast to the prominent role of the bed topography in the ice stream onset area [*Bell et al.*, 1998; *Anandakrishnan et al.*, 1998]. Measurements also suggest that the ice stream onset occurs atop several hundreds of meters to a kilometer thick layer of sediments, which apply an order of magnitude less frictional resistance to the ice above as compared to the material of the surrounding ridges [*Anandakrishnan et al.*, 1998; *Bell et al.*, 1998; *Peters et al.*, 2006]. Moreover, the ice-bed interface under the downstream section of ice streams can be substantially lubricated by meltwater and deformable sediments [*Kamb*, 1991; *Stokes et al.*, 2007].

[5] Various mechanisms have been examined with relation to the formation and spatiotemporal variability of ice

[1]Department of Applied Mathematics and Theoretical Physics, University of Cambridge, Cambridge, UK.
[2]Department of Earth and Planetary Science and School of Engineering and Applied Sciences, Harvard University, Cambridge, Massachusetts, USA.

0148-0227/11/2010JF001839

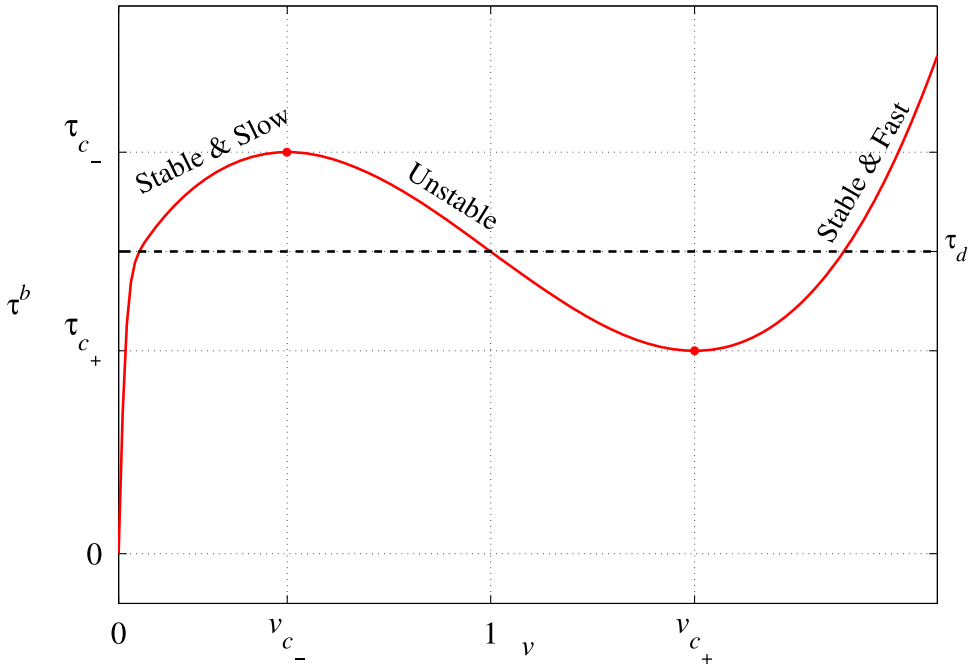

Figure 1. The triple-valued sliding law (or a cubic-like friction law) (ST2009) used in the present study. This friction law is composed of two linearly stable branches, slow ($v < v_{c\_}$) and fast ($v > v_{c+}$), and therefore can sustain stable flows of coexisting streams and interstreams.

streams. Thermoviscous effects were considered by *Payne* [1995], *Marshall and Clarke* [1997], *Payne and Dongelmans* [1997], *Hindmarsh* [1998], *Hulbe and MacAyeal* [1999], *Payne et al.* [2000], *Pattyn* [2003], *Saito et al.* [2006], and *Hindmarsh* [2009]. In particular, *Payne and Dongelmans* [1997] attributed ice stream variability to the competition over a common source, although these results may be model-dependent [*Payne et al.*, 2000]. Ice shear thinning rheology may be incapable to leading to spontaneous formation of ice streams through shear flow instability [*Sayag and Tziperman*, 2008]. Bed properties and conditions beneath the ice are believed to play a dominant role in the dynamics of ice flow [e.g., *Fowler*, 1986; *Tulaczyk et al.*, 2000; *Schoof*, 2004b, 2004a, 2006]. In particular, a triple-valued sliding law (similar to the one shown in Figure 1), was extensively studied in the context of glacier temporal variability and was shown to be useful for modeling glacier surging [*Lliboutry*, 1969; *Hutter*, 1982a, 1982b; *McMeeking and Johnson*, 1986; *Fowler*, 1986, 1987; *Greenberg and Shyong*, 1990; *Fowler and Johnson*, 1995; *Fowler and Schiavi*, 1998]. *Fowler and Johnson* [1996] showed that a triple-valued sliding law can lead to isolated domains of rapid flow, and suggested this as a possible mechanism for the development of ice streams. In a model that included horizontal shear stresses, *Sayag and Tziperman* [2009, henceforth ST2009] showed that a triple-valued sliding law (Figure 1) can lead to an ice-stream-like solution and account for both steady and time oscillatory behaviors (section 2). Note that a multivalued sliding law, which describes the sliding velocity as function of the basal stress, could also be described alternatively as a "cubic-like friction law," giving the stress as function of the sliding velocity.

[6] In this work we extend the study of ST2009 in two main directions. First, we investigate the effect of a non-Newtonian ice rheology on the spatial patterns of the flow under a triple-valued sliding law. Second, we study the spatiotemporal patterns of flow due to the interaction of two ice streams. For this purpose, we specify a transversely uniform mass source along the full width of the ice sheet surface at the upstream boundary. A specified topographic ridge constrains the ice to flow via one or two openings in the topography, creating one or two streams whose variability and interaction we study. We use numerical simulation with adaptive time step and spatial resolution of 2.5 km. This setup allows us to resolve idealized yet robust model solutions of coexisting ice streams and interstreams, and the shear margins in between, as confirmed by comparison with higher-resolution (1.25 km) simulations.

[7] The model and geometry used here are highly idealized, and we intentionally do not limit the parameter regime to a physically realizable one. Thus, this work does not attempt to realistically model ice streams, but rather attempts to study ice flow regimes motivated by observed ice streams and spanning a wider parameter range. This approach of exploring near-physical regimes, often results in interesting insights and is commonly used in bifurcation studies of geophysical systems [e.g., *Dijkstra*, 2000].

[8] By using the simplified dynamics and geometry, we are able to develop a relation between the parameters describing the ice rheology and the width of the model ice stream shear margins. We demonstrate how ice rheology affects the minimum sustainable ice stream width, as well as a lower bound on its maximum speed. Finally, we show the spontaneous symmetry breaking of a time oscillatory solu-

tion of two streams that is initially spatially symmetric. Specifically, as a result of an asymmetric initial perturbation to the ice thickness field, such a flow becomes spatially asymmetric, and gives rise to complex variability patterns such as the competition of two ice streams over a common source.

2. The Triple-Valued Sliding Law: Motivation and Possible Physical Mechanism

[9] A triple-valued sliding law relating the ice sliding velocity v to the bottom stress τ_b is shown in Figure 1. Note that for small velocities, $v < v_{c_-}$, the stress increases with velocity. For intermediate velocities, $v_{c_-} < v < v_{c_+}$, the stress decreases with the increasing velocity, and for larger velocities, $v > v_{c_+}$, the stress again increases with v. Such sliding laws have been used in particular in the context of surging glaciers [e.g., *Lliboutry*, 1969; *Fowler*, 1987], and *Fowler and Johnson* [1996] suggested that it may also account for ice streams.

[10] Measurements in the Siple Coast Whillans Ice Stream (originally ice stream B) show that the longitudinal component of velocity can drop from 400 m/yr to several meters per year across a narrow 4–5 km shear margin [e.g., *Echelmeyer et al.*, 1994]. In an effort to understand this transition ST2009 have assumed a unidirectional plug flow, Newtonian rheology and that the basal stress is a function of the ice velocity alone. Under these idealized assumptions one obtains a simple one-dimensional force balance, which in dimensionless form is

$$\varepsilon v_{,xx} + \tau_d - \tau_b(v) = 0, \tag{1}$$

where $v(x)$ is the plug flow velocity, x is the coordinate across that flow, $\varepsilon \ll 1$ is a dimensionless parameter representing the ratio of vertically-integrated horizontal shear stress to basal shear stress, and the terms on the LHS are horizontal shear stress divergence, driving stress (assumed constant), and basal shear stress, respectively. The structure of equation (1) indicates that the viscous shear stress divergence has negligible contribution to the force balance everywhere except in regions where divergence of strain rates is large, namely, where $v_{,xx} \sim 1/\varepsilon$. This implies that equation (1) can have solutions with boundary layers (shear margins) where sharp velocity gradients and concentrated stresses occur. Such concentrated shear stresses are hinted in observations of shear margins via the presence of crevassing. ST2009 showed that a triple-valued relation between the ice velocity and the basal shear stress, $\tau_b(v)$, is naturally motivated by equation (1), together with a nonuniform velocity profile representing an ice stream and an interstream ridge, coupled by a narrow shear margin.

[11] The triple-valued property of the sliding law permits two distinct and linearly stable modes of flow for the same basal drag: a fast one ($v > v_{c_+}$ in Figure 1) and a slower one ($v < v_{c_-}$). A stable flow velocity at a given position will become unstable if the basal shear stress at that position reaches one of the critical values, $\tau_{c_\pm}$. For example, starting with a flow velocity on the slower branch and corresponding basal stress, τ_b, a small increase in the applied driving stress can increase the flow velocity slightly if $\tau_b \ll \tau_{c_-}$, but will lead to a significant amount if $\tau_b = \tau_{c_-}$. In addition, these two modes of flow can coexist in a bistable state of flow (motionless margins) or an unstable state (margins move toward the ice stream center or away from it). These stability properties of the friction law may change in more complicated 3-D ice flows. When the dynamics of model ice streams are dominated by a triple-valued sliding law, ST2009 find that there is no preferred ice stream width, and the model stream width is then found to be controlled by external factors such as the rate and distribution of snow accumulation.

[12] Numerical simulations with an ice sheet model that includes membrane stresses (shelf stream approximation) with a triple-valued sliding law similar to Figure 1 show solutions of both a steady ice stream over a uniform bed, and a periodically surging ice stream (ST2009). This suggests that the physical mechanism of ice streams and surges may be related, as also proposed earlier by *Weertman* [1964] and *Fowler and Johnson* [1996]. Mechanisms that were proposed to explain glacier surging, such as the reorganization of the subglacial drainage system [e.g., *Walder*, 1982; *Kamb et al.*, 1985; *Kamb*, 1987; *Fowler and Johnson*, 1996; *Raymond*, 2000] or related mechanism that results in bimodal flow states [e.g., *MacAyeal*, 1993a; *Tulaczyk et al.*, 2000], are also potential candidates to account for ice streams. More specifically, the triple-valued sliding law may be rationalized following these references as follows: at low sliding velocities ($v < v_{c_-}$), meltwater production is at low rate and effectively drained, leading to an inefficient lubrication and large basal stress. At faster sliding velocities ($v_{c_-} < v < v_{c_+}$), drainage rate is insufficient to balance meltwater production, leading to efficient lubrication and reduced friction. Finally, at yet higher sliding velocities ($v > v_{c_+}$) low-pressure channels may form close to the ice stream center, and drain subglacial water effectively, leading again to an increase in basal stress (similar principle to "drainage limited" stability [*Raymond*, 2000]).

[13] A critical element of the triple-valued sliding law is therefore the faster branch ($v > v_{c_+}$), which allows a *fast* and *stable* flow regime and therefore a steady ice stream solution, in contrast to a "runaway" situation. This triple-valued structure also leads to roughly similar basal shear stresses near the ice stream center and in interstream regions far from shear margins, where they are of the order of the driving stress, τ_d. Basal shear stress near the shear margins, where horizontal shear stresses are important, can be significantly smaller than the driving stress (Figure 1) (ST2009, Figure 8). In reality, basal shear stress in the vicinity of the ice stream center may be smaller than that at the interstream far from the margin, due to processes that the idealized model of ST2009 does not include.

[14] The subglacial processes mentioned above were not explicitly included in the triple-valued sliding law of ST2009. Nevertheless, it was suggested there that it may be possible to account for some of the observed ice stream features using any other basal processes which lead to a triple-valued relation between ice velocity and basal shear stress.

3. The Model

[15] Consider the flow of ice of density ρ and constant temperature, within a rectangular domain. The two horizontal coordinates are x (transverse to the mean flow) and

y (along the mean flow), and z is the vertical coordinate. The ice force balance is derived under the assumptions that the basal shear stress is much smaller than the ice viscous stresses, which leads to plug flow; that the ice sheet ratio of the vertical to horizontal length scales, $[h]/[L]$, is small (see notation section); and incompressibility. Under these assumptions, the three-dimensional Stokes equations can be approximated to leading order as a horizontal plain flow (shelf stream approximation) [*MacAyeal*, 1989],

$$0 = \left[2\mu h\left(2u_{,x} + v_{,y}\right)\right]_{,x} + \left[\mu h\left(u_{,y} + v_{,x}\right)\right]_{,y} - \rho g h (h+b)_{,x} - \tau_b^x, \tag{2}$$

$$0 = \left[\mu h\left(u_{,y} + v_{,x}\right)\right]_{,x} + \left[2\mu h\left(u_{,x} + 2v_{,y}\right)\right]_{,y} - \rho g h (h+b)_{,y} - \tau_b^y. \tag{3}$$

Variables and parameters are defined in the notation section. The velocity field is given by $\boldsymbol{v} = u\boldsymbol{x} + v\boldsymbol{y}$, where $\boldsymbol{x}, \boldsymbol{y}$ are unit vectors in the horizontal coordinate directions, and μ is the effective viscosity governed by a power law viscous constitutive relation [e.g., *Hutter*, 1983],

$$\mu = \frac{1}{2} A^{-\frac{1}{n}} \left(\frac{\dot{\epsilon}_{II} + R}{1+R}\right)^{\frac{1}{2}\left(\frac{1}{n}-1\right)}. \tag{4}$$

The ice stiffness parameter, A, is an Arrhenius function of the temperature and of the activation energy; $\dot{\epsilon}_{II} = u_{,x}^2 + v_{,y}^2 + u_{,x}v_{,y} + \frac{1}{4}\left(u_{,y} + v_{,x}\right)^2$ is the leading-order approximation of the second invariant of the strain rate tensor; and n is the flow law exponent. Typically, $n > 1$, suggesting that the model ice behaves as a shear thinning fluid (reduction of effective viscosity with increased rate of strain), and therefore requires a regularizing parameter, R, that is introduced into equation (4) [e.g., *Hutter et al.*, 1981]. We choose $\log_{10} R = -28$ by matching equation (4) with rheological experimental data of *Barnes et al.* [1971] [*Sayag*, 2009]. Below, we study the flow in a range of the rheological parameters n and A that is within the experimental uncertainty [e.g., *Barnes et al.*, 1971; *Goldsby and Kohlstedt*, 2001].

[16] The ice thickness is $h(x, y, t) = s - b$, where $z = s(x, y, t)$ is the ice surface and $z = b(x, y)$ is the bed topography, which is specified as a ridge that separates the mass source area upstream from a flat downstream region. The ridge has either a single opening (Figure 2a) or two openings (Figure 10a) and is specified as

$$b(x,y) = b_0 \sum_j \exp\left[-\left(\frac{x - x_j}{\sigma_{x_j}}\right)^{q_j} - \left(\frac{y - y_0}{\sigma_y}\right)^2\right], \tag{5}$$

where the number of exponents in the sum over j determines the number of openings in the topography, and the related parameters are specified in Table 1. Such bed topography allows us to control the outflow of the mass source and therefore the number, and to some degree the maximum width, of the ice streams, as further discussed below. As explained in the introduction, this geometry is not meant to realistically simulate the Siple Coast topography, but to allow us to control the number and location of ice streams and to study their interaction.

[17] The cubic-like friction law (section 2) used to calculate the bottom shear stress, $\boldsymbol{\tau}_b = (\tau_b^x, \tau_b^y)$, is a critical element of this study and is based on the one used by ST2009 (Figure 1),

$$\boldsymbol{\tau}_b = \frac{[\tau_b]}{[v]} \frac{\boldsymbol{v}}{\vartheta}\left((\vartheta - 1)^3 + a(\vartheta - 1) + 1 + b(x,y)/b_0\right) \tanh(\beta\vartheta), \tag{6}$$

where $[v]$ is the velocity scale, $[\tau_b]$ is the basal shear stress scale, $\vartheta = |\boldsymbol{v}|/[v]$ is the nondimensional magnitude of the velocity, and where the parameters a and β are chosen such that the slow and fast velocity regimes are similar to those observed (see notation section). The friction term b/b_0, is introduced to account for the observed larger friction due to subgrid-scale bottom roughness in ice stream onset regions of prominent bed topography (see references in section 1), with the purpose of artificially forcing the ice to flow primarily via the opening(s) in the basal topography.

[18] Conservation of mass implies

$$h_{,t} = M - (uh)_{,x} - (vh)_{,y}, \tag{7}$$

where the specified net accumulation rate, M, is prescribed to be independent of x,

$$M(y) = M_0 \exp\left(-y^2/\sigma_m^2\right), \tag{8}$$

and where M_0 is the mass source intensity (Tables 2 and 3). Note that the large and unrealistic values of the mass accumulation source, here specified over a small area of the domain, are meant to represent smaller accumulation rates over larger upstream areas in reality.

[19] The model we use is based on assumptions that may not hold in regions where vertical shear or thermal effects on creep become of leading importance, such as in the onset regions. However, we argue that the triple-valued sliding law is the key dynamical component responsible for the results we show below, and that the above processes would only affect these results quantitatively, as further discussed in section 6.

[20] We use finite difference to discretize the force and mass balance equations on a staggered grid. The domain size is 250 km by 250 km, with 2.5 km or 1.25 km grid spacing. The diagnostic and nonlinear force balance equations and the effective viscosity field are iteratively solved simultaneously using Picard iteration with a subspace correction [*Hindmarsh and Payne*, 1996] to cope with the high-velocity shear. The time-dependent mass balance equation is integrated using an adaptive time step approach, with time step ranging from 1 min to 12 h. The boundary conditions on the domain sides, $x = 0$, 1, are periodic, while the upstream boundary at $y = 0$ is free slip ($\tau_{xy} = 0$) and allows no normal flow ($v = 0$). The down stream boundary conditions are based on the outflow condition suggested by *Papanastasiou et al.* [1992], which is essentially an upwind difference scheme near the boundary. However, this condition is insufficient since the solution becomes numerically unstable as the shear margin front approaches the outflow boundary. We overcome this problem by adding the condition $v_{,y} = 0$ at the outflow, $y = 1$. Computations are performed with Intel FORTRAN using parallel sparse direct

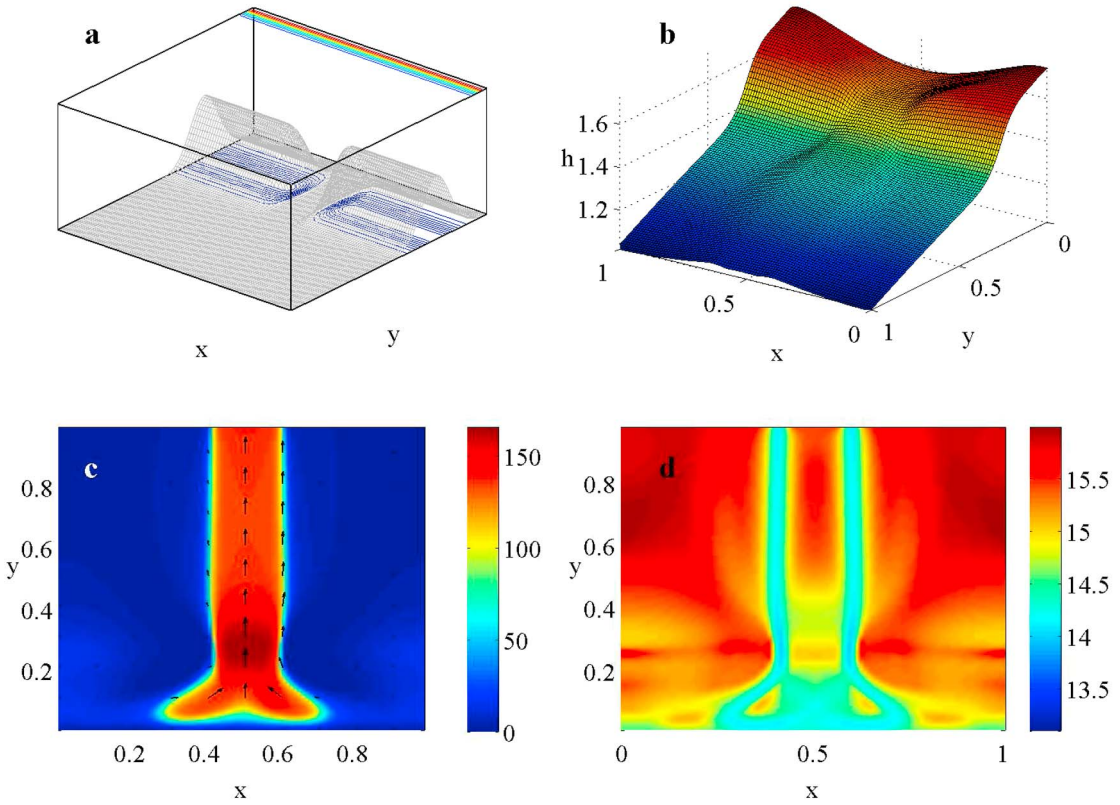

Figure 2. Simulation results for a single ice stream in steady state (run 1e, Table 2). (a) Geometry. The ice flows over a plane through an opening in the center of an upstream ridge. The mass source is distributed uniformly in x farther upstream of the ridge (color contours, red is higher than blue). (b) Ice thickness (nondimensional). Thickness gradients of the ice are maximal upstream, around the region of the bottom topography ridge. (c) Color contours of the velocity magnitude (meters per year) and velocity arrows of an ice stream solution, showing the region of fast flowing ice (red). Arrows are plotted every ten grid points. (d) Effective viscosity ($\log_{10}\mu$), showing values that are ~3 orders of magnitude smaller in the shear margins than in the interstream regions.

solver, PARDISO. The numerical model is presented thoroughly by ST2009, where a constant viscosity μ was assumed.

4. Analysis of a Single Stream Scenario

4.1. Shear Margin Width

[21] We start by analyzing the factors that determine the width of the ice stream shear margins in this model. The shear thinning rheology of ice implies that where the shear rate is larger, the effective viscosity is lower. This effect is clearly reflected in simulation results where a steady ice stream develops (Figure 2). The model ice stream emerges downstream from the opening in the ridge (Figure 2c) and has narrow yet clear shear margins that separate the region of fast and slow flow. The effective viscosity in the shear margins is about three orders of magnitude smaller than at the center of the stream or in regions outside of the stream, indicating significant shear thinning (Figure 2d).

[22] The extent of shear thinning depends on the rate of shear and also on the parameters n and A in equation (4). The effect of these parameters on the width of an ice stream shear margin can be estimated directly from equation (3) to

Table 1. Bed Topography Parameters[a]

Parameter	One Gap	Two Gaps
J	2	3
q_j	32, 32	32, 32, 32
x_j	0, 1	0, 1/2, 1
σ_{xj}	0.42, 0.42	24, 14, 24
σ_y, y_0	10, 0.25	10, 0.25

[a]See equation (5).

Table 2. One-Gap Simulations[a]

Run	n	$\log_{10} A$	M_0(m/yr)	$\Delta x(y = 0.7)$ (km)	Variability
1a	2	−19.6	7	7.71	steady
1b	2	−20.2	6	11.6	oscillatory
1c	2	−21.1	10	24	steady
1d	2	−21.1	8	26.4	oscillatory
1e	3	−24.0	7	5.22	steady
1f	3.15	−26.3	7	11.95	steady
1g	3.15	−26.3	6	13.1	oscillatory
1h	3.15	−26.5	9	13.3	steady
1i	4	−30.4	8	8.9	steady
1j	5	−34.9	7	7	steady

[a]Velocity and basal shear stress scales are $[v] \simeq 70$ m/yr and $[\tau_b] \simeq 63$ KPa.

Table 3. Summary of the Results of the Two-Gap Simulations With Symmetric Initial Conditions[a]

Run	n	$\log_{10} A$	M_0 (m/yr)	$\Delta x(y = 0.7)$ (km)	Period (years)	Stream (years)
2a	2	−20.2	10	11.5	65.27	30.65
2b	2	−19.9	10	10.5	56	27.3
2c	2	−19	10	5.38	steady	steady
2d	3.15	−26.3	10	12	83.17	36.85
2e	4	−30.5	10	10.5	78.7	37.3

[a]"Period" refers to the period of the oscillation and "stream" is the duration of the active phase of the rapid flow within the period. Velocity and basal shear stress scales are $[v] \simeq 70$ m/yr and $[\tau_b] \simeq 63$ KPa.

within constant factors that can be evaluated numerically. Neglecting variations of the flow field in y and assuming $u \ll v$ and $u_{,x} \ll v_{,x}$, equation (3) becomes

$$0 = \left[\mu h v_{,x}\right]_{,x} - \rho g h (h+b)_{,y} - \tau_b^y. \tag{9}$$

Substituting $\mu = (1/2)A^{-1/n}|v_{,x}|^{1/n-1}$, we find that the interval Δx, representing the shear margin width across which the velocity drop is Δv, is given by,

$$\Delta x = \left(\frac{[h]/2}{\rho g [h]^2/[L] + [\tau_b]}\right)^{\frac{n}{1+n}} \left(\frac{\Delta v}{A}\right)^{\frac{1}{1+n}}. \tag{10}$$

[23] The choice of Δv is motivated by the friction law, which defines the slowest stable velocity a rapid stream can have (v_{c_+}), and the fastest stable velocity an interstream (slow) region can have (v_{c_-}) (ST2009). These are defined as the local maximum and minimum of the basal shear stress and, from equation (6) and Figure 1, can be evaluated to a very good approximation as,

$$v_{c_\pm} \simeq 1 \pm \sqrt{|a|/3}, \tag{11}$$

where in equation (6), $\tanh(\beta\vartheta) \simeq 1$ (see notation section) and where the term b/b_0 vanishes in the absence of topography. We therefore choose $\Delta v = v_{c_+} - v_{c_-}$ to represent the drop in velocity across the shear margin. To evaluate the validity of equation (10) we let the numerical simulation converge to a steady state ice stream for several sets of the parameters n and A (Table 2), and measure the shear margin width, defined as the interval

$$\Delta x \equiv \left|x(v = v_{c_+}) - x(v = v_{c_-})\right|, \tag{12}$$

across which the drop in velocity is Δv (Figures 3a and 3b). We then fit the simulation data to a function of the form,

$$\Delta x(n, A) = c_1^{\frac{n}{1+n}} \left(\frac{c_2}{A}\right)^{\frac{1}{1+n}}, \tag{13}$$

and use least squares to solve for the unknown parameters, $c_{1,2}$,

$$c_1 \simeq 4.72 \left(\frac{[h]}{\rho g [h]^2/[L] + [\tau_b]}\right), \qquad c_2 \simeq 2.10 \Delta v. \tag{14}$$

Figure 3a shows that equation (13) predicts fairly well the shear margin width for the specific model we consider here. We can now use the functional relation (13) to evaluate the shear margin width as function of the rheology parameters n and A. Figure 4 shows that a particular shear margin width, Δx, is consistent with a continuous range of values for n and A. The choice of a specific value for n and A will affect the magnitude of the effective viscosity and, as we show below, the evolution and character of the flow. Other physical mechanisms, not considered here explicitly, may also be a factor in explaining the shear margin width (e.g., strain-induced anisotropy) [*Echelmeyer et al.*, 1994; *Truffer and Echelmeyer*, 2003].

4.2. Analyzing the Stagnation of an Ice Stream

[24] The ice-stream-like pattern generated under the friction law (equation (6)) may be arbitrarily wide, limited only by the availability of a mass source that can sustain it (ST2009). As the mass accumulated in the source region is exhausted, the driving stress due to the surface slope

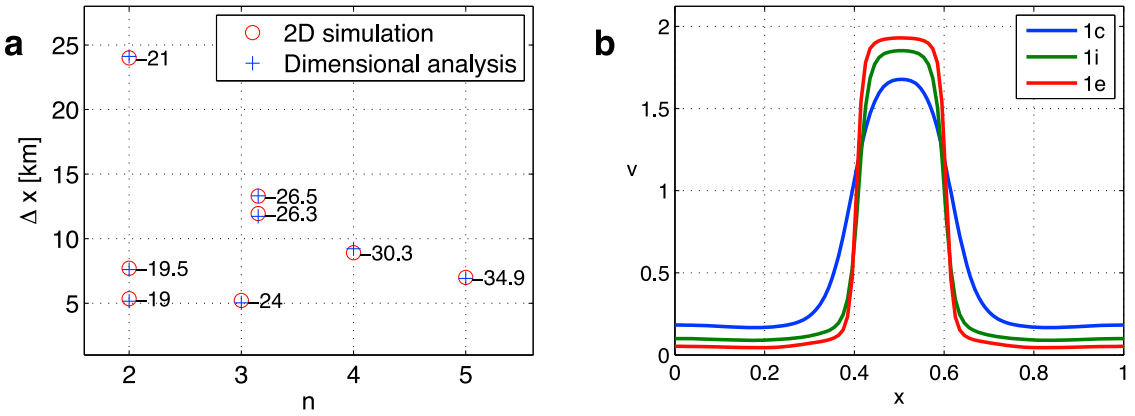

Figure 3. Shear margin width from several different model runs, as a function of the ice rheology parameters, n (x axis) and $\log_{10} A$ (numbers beside markers). (a) The predicted values based on equation (13) (crosses) and the results of the 2-D simulation (circles). (b) A cross section of the downstream velocity, v, at $y = 0.5$, for selected parameters n, A in Figure 3a (Table 2).

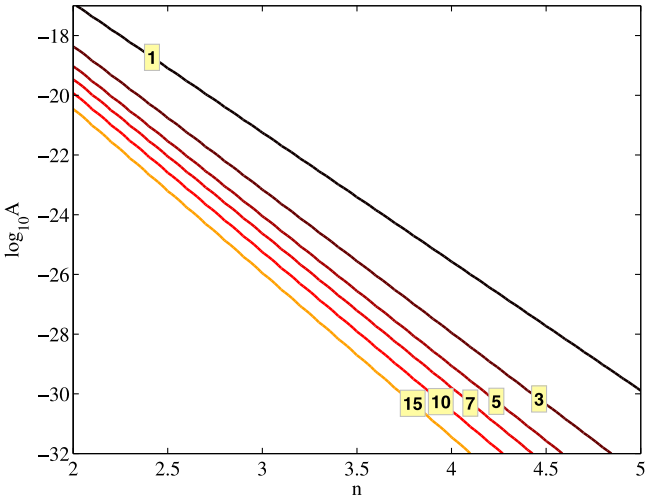

Figure 4. A contour plot of the shear margin width, Δx (kilometers), as a function of the ice rheology parameters, n and $\log_{10} A$, based on equation (13).

diminishes and the stream narrows until it reaches a critical width and stagnates. This behavior can occur periodically under a time-independent mass source as seen in the Newtonian fluid simulations of ST2009. We observe a similar behavior for the non-Newtonian rheology and the particular bed structure in Figure 2a, yet the more general configuration used here allows for several new and different modes of rapid flow for a given mass source distribution, M (Figure 5). One mode is a temporary fast flowing ice-stream-like region, enclosed within a slower flowing region, that does not grow all the way to the outflow boundary before stagnation (Figure 5b). A second mode occurs when the fast flowing region propagates to and breaks through the downstream boundary to form an ice stream (Figure 5c). A third mode occurs when the driving stress is sufficiently large to drive the flow into the rapid regime throughout most of the upstream region and all of the downstream region (Figure 5d).

[25] These different modes all occur within the same model run in a seemingly aperiodic manner. The behavior seems chaotic in time, although the length of the time series, limited by computational cost, does not allow us to verify this. Some of these features are clearly not realistic and likely to be due to the idealizations used in our model and friction law. But these results do demonstrate the rich behavior supported by this simple model and sliding law, and some of these modes may be relevant to the observed behavior of the Siple Coast ice streams.

[26] Once an ice stream is formed, its shear margins migrate inward until it reaches a certain width, and then the ice stream becomes stagnant abruptly (at ~50 km in Figure 5c).

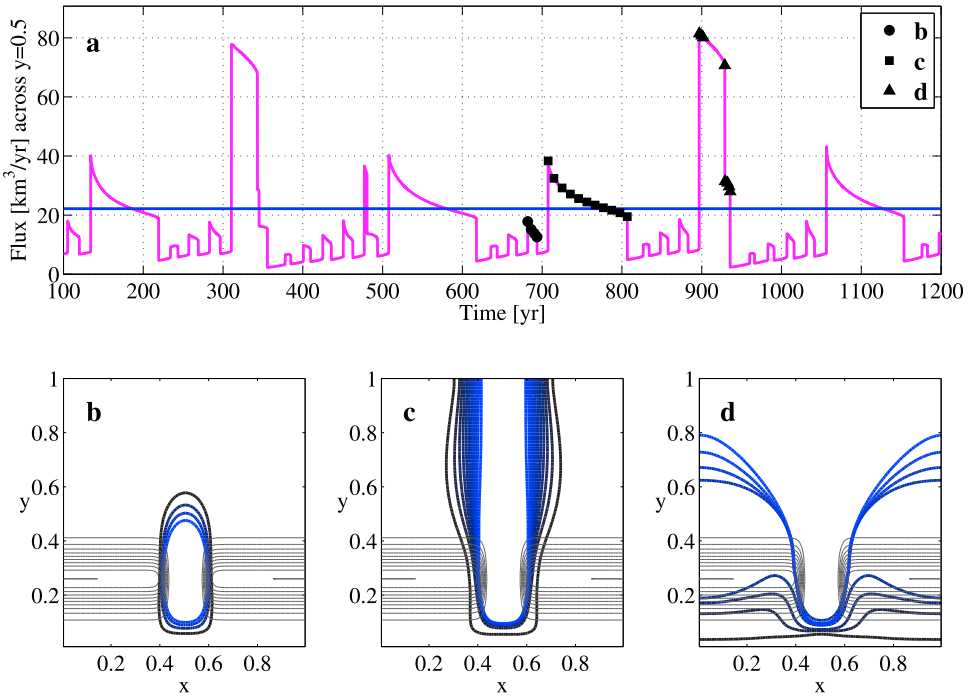

Figure 5. Different regimes of a single ice stream solution. (a) A time series of the integrated mass flux across $y = 0.5$ (run 1d, Table 2). Three distinctive patterns of flow are apparent in the time series and correspond to the different spatial patterns in Figures 5b–5d via the $v = 1$ contour which roughly marks the shear margin position. (b) A locally confined fast flow pattern that does not penetrate all the way to the downstream outflow boundary. Contoured snapshots correspond to the short-time-scale, small-amplitude oscillation denoted by full circle symbols in Figure 5a. Darker contours refer to earlier times. (c) Snapshots of the ice-stream-like solution during the long-time-scale oscillations (squares in Figure 5a). (d) Patterns of unconfined fast flowing region during the short-time-scale, large-amplitude oscillations denoted by triangles in Figure 5a.

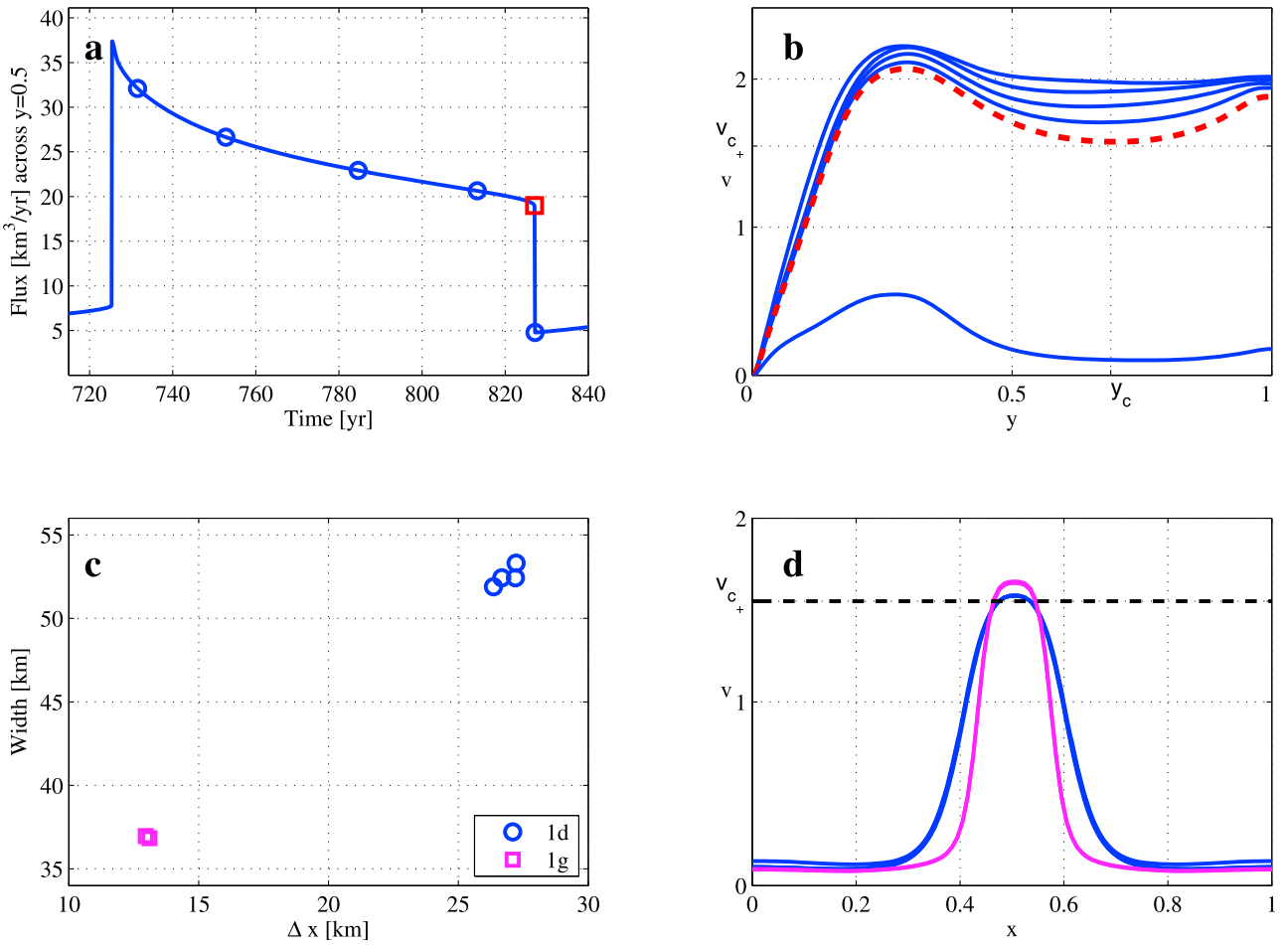

Figure 6. Analysis of the critical state of an ice stream, just before stagnation. (a) A time series of the total mass flux across $y = 0.5$ during a development and stagnation of an ice stream (run 1d, Table 2). The ice stream width declines with its mass flux. (b) The downstream velocity, $v(y)$, along the ice stream center, at times marked by circles in Figure 6a. The value v also declines with the mass flux but remains stable as long as $v > v_{c_+}$. When $v \approx v_{c_+}$, (square in Figure 6a and dashed curve in Figure 6b) the ice stream becomes stagnant. (c) A demonstration that the critical width of an ice stream just before stagnation is a function of the shear margin width. Shown is the ice stream width just before stagnation, as a function of the shear margin width Δx (equation (13)). Circles denote four stagnation events in run 1d, and squares denote two stagnation events in run 1g (Table 2). These two runs differ in the values of n and A, showing that for a given value of the rheology parameters the critical width of the ice stream is nearly constant. (d) A typical cross section of the downstream velocity v at $y = y_c$ in Figure 6b, just before stagnation (runs 1d and 1g).

The migration rate inferred from Figures 5a and 5c is ~250 m/yr, consistent with observations within an order of magnitude. The critical state of a rapid flowing ice stream just before stagnation, and in particular the maximum velocity and width, can be characterized using the friction law (equation (6) and Figure 1). Simulation results (Figure 6) show that just before the stagnation, the minimum downstream velocity v at the downstream part of the ice stream, is just above v_{c_+}. At that instant, the stream width is narrower in model runs for which the shear margin width is narrower (Figures 6c and 6d), providing insight into the stagnation mechanism of the ice streams in this model: a stagnation occurs when the ice stream width is about twice the shear margin width, or, put more crudely, when the two shear margins, as per our definition (equation (12)), first touch. For example, Figure 6c shows that the shear margin width before stagnation is 27 km while the ice stream width (also per our definition) at that point is 53 km. This implies that before stagnation the ice stream narrows to a width of the order of tens of kilometers where it quickly becomes stagnant. This stagnation process of ice streams in our model seems qualitatively consistent with that of Kamb Ice Stream (originally ice stream C), which narrowed by 30% before a rapid stagnation at a final width of ~75 km (averaging along the interval between the grounding line and ~200 km upstream) [*Catania et al.*, 2006; *Jacobel et al.*, 2000].

4.3. Transient and Asymmetric Behavior of the Upstream Flow

[27] As expected, the flow from the mass source region to the downstream area tends to concentrate in the gap through the bottom topography ridge. Although the mass source is

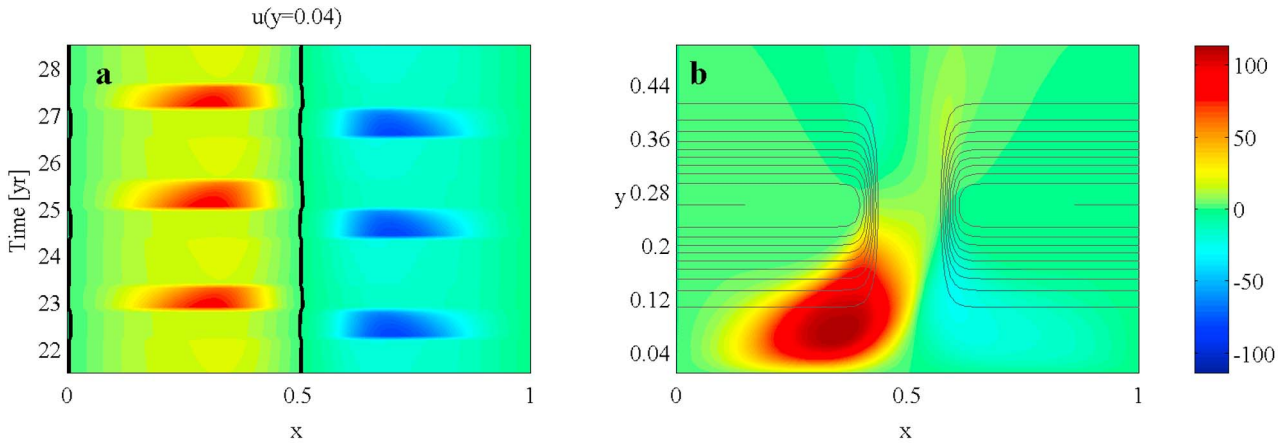

Figure 7. The transverse flow pattern at the upstream part of the domain (run 1f, Table 2). (a) The transverse velocity, u at $y = 0.04$ as a function of time and x, showing an upstream flow that is asymmetric with respect to $x = 0.5$, with flushes of rapid transverse flow alternating from side to side. (b) A snapshot of the transverse flow (u) at the upstream region and contours of the bottom topography. Color bar refers to both Figures 7a and 7b.

uniformly spread along the upstream boundary, and the bed topography and roughness are also symmetric with respect to the gap center at $x = 0.5$, the transverse component of the velocity u in the upstream region can become asymmetric (Figure 7). As mass is accumulated in the source area, transverse surface slopes build up (red regions in Figure 2b). Over time, the transverse driving stress can reach a critical value where u becomes larger than the friction law critical velocity v_{c-} and a region of rapid flow develops. Such a flush event is active on one side of the gap for ~1 year, and then ceases for another half year, before a new flush event initiates on the other side of the gap, creating a cycle with a period of about 3 years (Figure 8a). This behavior is absent for some rheological parameter combinations (e.g., $n = 2$, $\log_{10} A = -21.1$; run 1c, Table 2) that lead to a more viscous flow in the upstream region and for which transverse surface slopes in the upstream region do not build up sufficiently.

[28] The occurrence of an upstream flush slightly increases the mass flux in the downstream regions (Figure 8a). As a result, the ice stream width (measured for this purpose as the width of the downstream velocity contour $v = 1$ in dimensionless units) varies with a small amplitude between 37.8 and 38.9 km and the maximum downstream speed varies approximately between 124.7 and 125.8 m/yr.

[29] The transverse velocity flushes also transport mass from one half of the domain (e.g., $x < 0.5$) to the other half (e.g., $x > 0.5$) (Figure 9). The transverse mass flux across the interface $x = 0.5$ occurs mostly in the mass source area, for $0 < y \lessapprox 0.3$. Further downstream, there is hardly any mass flux exchange between the two domain halves.

[30] We observe the transverse flushes described above in higher-resolution simulations (grid spacing 1.25 km) as well, which indicates that their presence is due to the model dynamics rather some numerical artifacts. In particular the asymmetric behavior of the upstream flow could be a result of a spontaneous symmetry breaking due to the nonlinear nature of the system (as is typical for example in simpler dynamical systems undergoing a pitchfork bifurcation) [*Strogatz*, 2001]. That is, the symmetric solution becomes linearly unstable to small perturbations and the system switches to an asymmetric state. However we do not feel these flushes are necessarily relevant to the onset area of observed ice streams as our representation of the upstream area is less adequate than in other parts in the flow domain. Specifically, our model neglects vertical shear and the complex topography in observed onset areas, and the mass source distribution is not realistic. Nevertheless, we still find it interesting that the model dynamics allows for the rich dynamics of intermittency, asymmetry and "flushing" behavior, even if this tells us more about what the physics included in the model is capable of, than about the specific dynamics of the Siple Coast ice stream onset area.

5. Interaction of Two Streams

[31] To study the interaction between two adjacent streams we introduce two gaps into the prescribed bottom topography ridge separating the source region from the downstream region (Figure 10a and Table 1 with $j = 3$). Again, the flow from the mass source area is concentrated in the gaps in the basal topography, driven by transverse surface gradients (Figure 10b). We analyze the flow pattern over this topography in a set of simulations with the rheological parameters shown in Table 3. We focus on describing several interesting features and issues that arise in the numerical solutions: (1) the different flow patterns that form, (2) factors leading to independent versus merging streams, (3) the destabilization of spatially symmetric solutions, and (4) the role of non-Newtonian rheology.

5.1. Flow Patterns in the Presence of Two Adjacent Streams

[32] The flow pattern in the presence of two gaps in the bed topography and with a constant mass source intensity strongly depends on the rheological parameters that determine the shear margin width (section 4.1 and Figure 4) and on the critical velocities associated with the basal friction law (equation (11)). Depending on these parameters, the

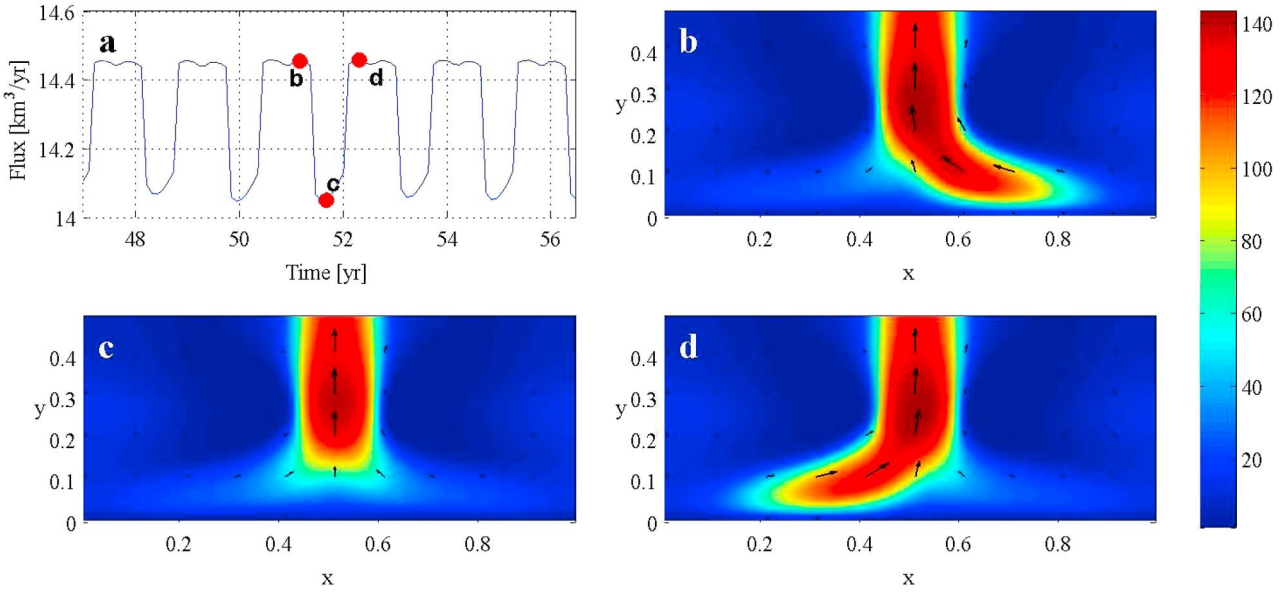

Figure 8. The effect of the upstream flushes on the downstream flux pattern of an ice stream (run 1b, Table 2, which converges to a statistically steady state). (a) The mass flux across $y = 0.5$ versus time (years) (pattern continuous indefinitely). (b–d) Snapshots of the upstream velocity field corresponding to times marked by the three full circles in Figure 8a (color values in meters per year).

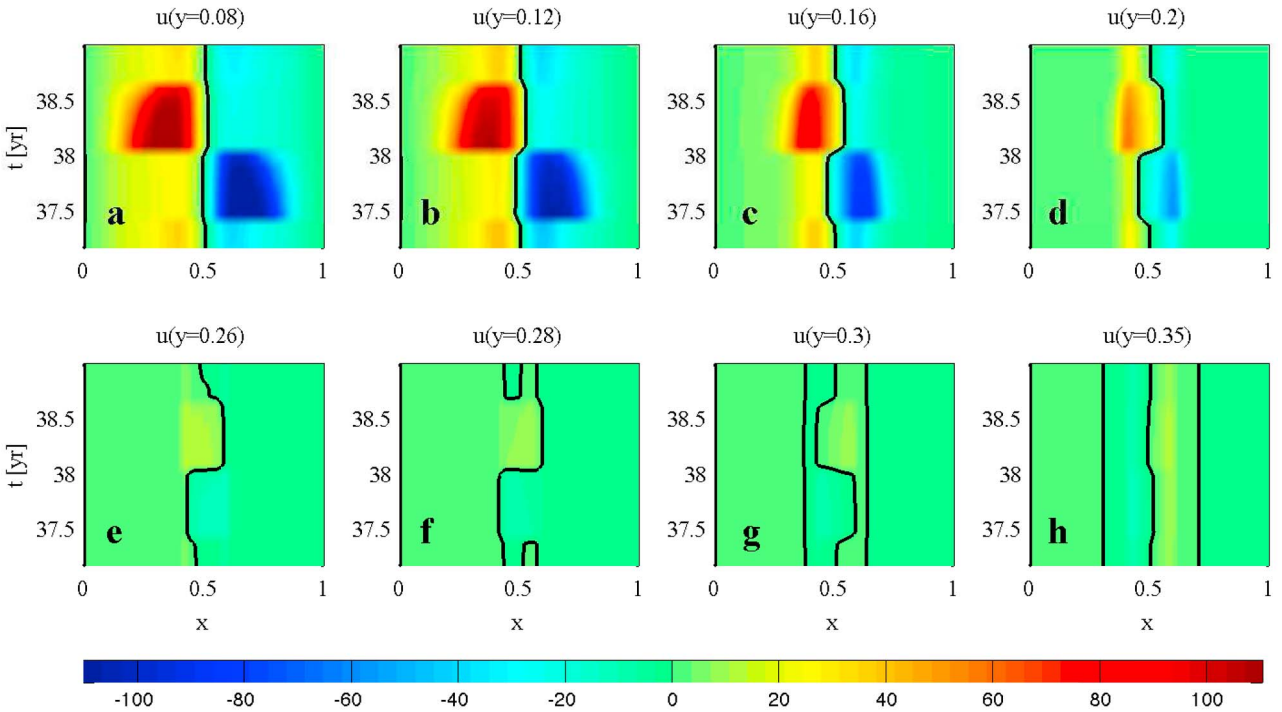

Figure 9. Contour plot of the transverse velocity u as a function of time and x, at several upstream positions, y, showing that there is a flow crossing from one half of the domain (e.g., $x < 0.5$) to the other half for $0.08 < y < 0.3$. The y position is noted at the top of each frame. Note that the direction of the flow across the center of the domain alternates in time. Color values are in meters per year, and the black contour is $u = 0$.

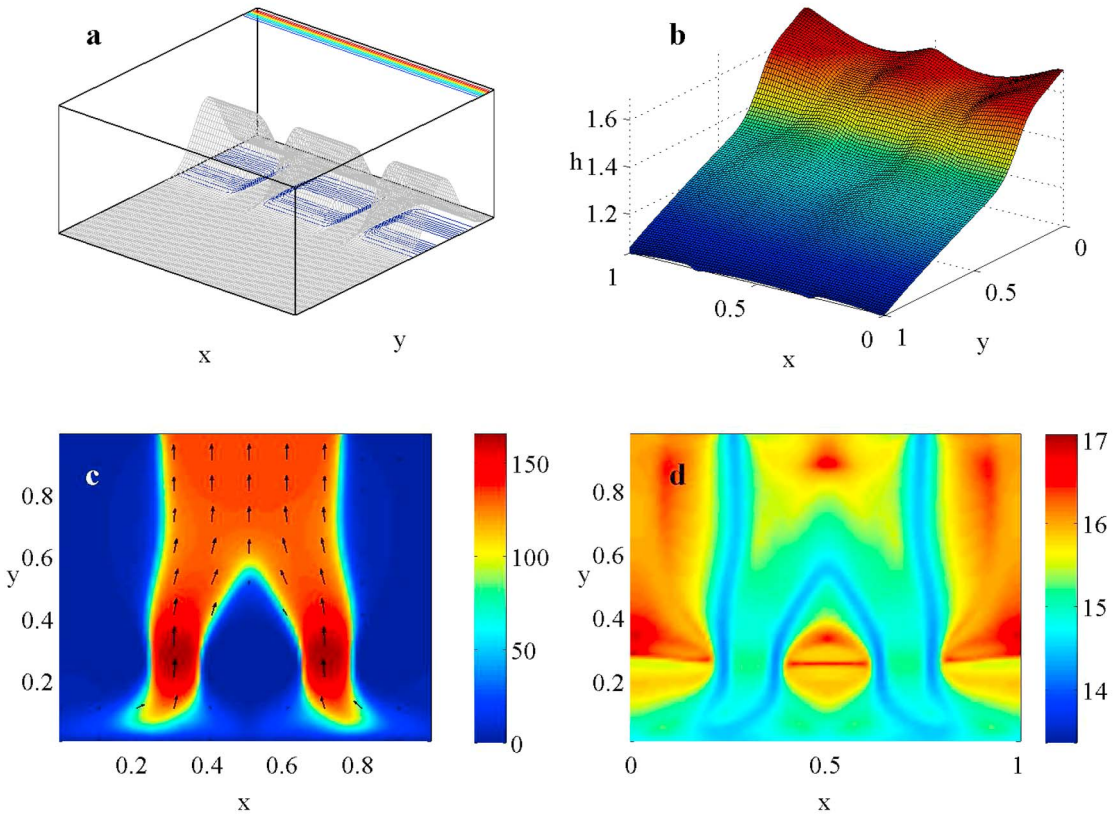

Figure 10. Simulation results for a bottom topography with two openings (run 2d, Table 3). (a) Geometry. The ice flows over a plane through two openings in an upstream ridge. The mass source is distributed uniformly in x farther upstream of the ridge (color contours, red is higher than blue). (b) Ice thickness (nondimensional). Thickness gradients of the ice are maximal upstream, around the region of the bottom topography ridge. (c) Color contours of the velocity magnitude (meters per year) and velocity arrows of an ice stream solution, showing the region of fast flowing ice (red). Arrows are plotted every ten grid points. (d) Effective viscosity ($\log_{10}\mu$), showing values that are ~3 orders of magnitude smaller in the shear margins than in the interstream regions.

flow may arrange to form a single stream fed by both openings in the topography (Figures 10c, 12a, and 12b), two separate steady streams (Figure 11a), or asymmetric streams that alternate active phases with seemingly chaotic behavior in time (Figures 12c, 12d, and 13).

[33] Consider first the issue of two separate streams versus the merging of two streams into a single wide stream. When the shear margins are sufficiently narrow (e.g., run 2c in Table 3), the flow can reach a steady state with two separate streams emanating from the two bed topography gaps (Figure 11a). As the rheological parameters are changed and the shear margins widen, the margins of the two streams approach each other (Figure 11b). Model simulations reveal a simple picture: as the margins of the two streams approach, the slow flow in between them speeds up due to horizontal shear stresses with the relatively faster flow to either side. When the flow velocity in the interstream region reaches the critical velocity v_{c_-}, it is in the unstable range shown in Figure 1, and its speed increases to over v_{c_+} before it stabilizes again, leading to merging of the two streams to a single wide one. It is clear that the minimum stable width of the inter stream between two initially isolated and adjacent streams, decreases as the shear margin width decreases.

[34] Once the two streams merge into a single wider stream (Figure 10c), the downstream mass flux increases substantially. The upstream mass source cannot sustain this large mass flux in a steady state and, as a result, the streams eventually separate again. This can result in an oscillatory behavior where two streams combine and then separate repeatedly (Figure 12a). The separation of the streams occurs via the downstream movement of the point at which the two streams merge downstream of the topographic gaps ($(x, y) = (0.5, 0.55)$ in Figure 10c).

[35] This merging of two streams and the splitting of a wider stream demonstrate that there is no inherent width scale for ice stream solutions due to the triple-valued sliding law (ST2009). The sliding law allows the two regimes of fast and slow flow to coexist, and the only limit on the maximum width of the fast flow domain is the availability of a mass source that can sustain it.

5.2. Spontaneous Symmetry Breaking of the Interaction Pattern

[36] If the model is initialized with initial conditions that are symmetric with respect to the two gaps in the topography, the solution remains symmetric for long periods of time

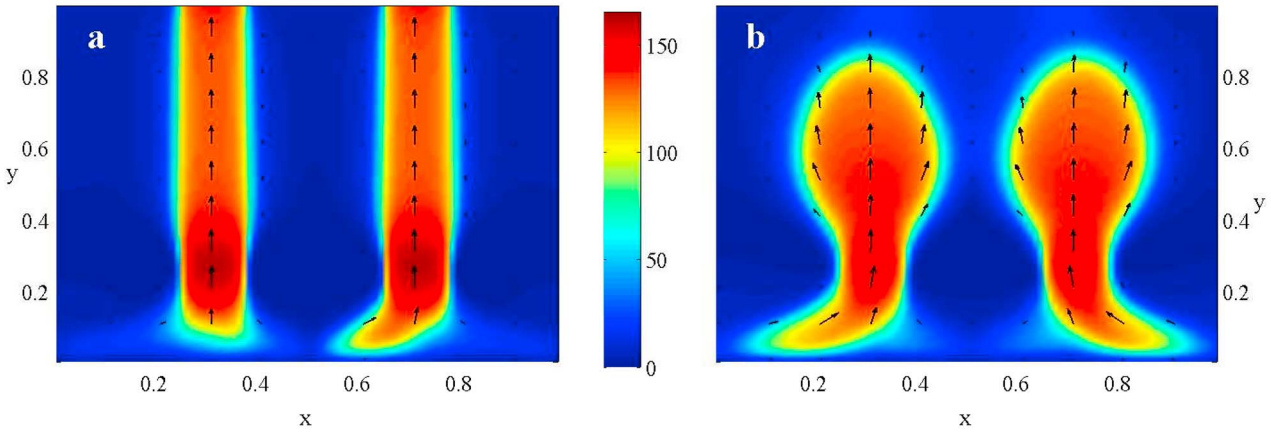

Figure 11. Different patterns of interaction of spatially symmetric ice streams. Shown are the magnitude of the ice flow speed (colors, meters per year) and the flow directions (vectors, plotted every 10 grid points). (a) A model simulation for which Δx = 5.4 km, showing that the streams can remain separated (simulation 2c, Table 3). (b) A model simulation where Δx = 10.5 km, showing the streams approaching each other to within a critical distance (run 2d, Table 3) that can lead to their merging (Figure 10c).

even with time-dependent, oscillatory solutions of merging and separating ice streams (as described above and shown in Figures 12a and 12b). It turns out, however, that for a fairly wide range of rheological parameters, this initially symmetric solution is unstable and can undergo spontaneous symmetry breaking: applying a small asymmetric ice thickness perturbation to an initially symmetric model simulation leads to a complex, seemingly chaotic, asymmetric flow pattern (Figures 12c, 12d, and 13). The perturbation introduces a temporal phase difference between the two ice streams which is then sustained by the dynamics.

[37] Specifically, the upstream driving stresses in the domain half where a thickness perturbation is introduced (e.g., $x > 0.5$) reaches the critical value leading to ice stream formation earlier than the other half (Figure 13b). That initial ice stream consumes part of the mass source in the $x < 0.5$ half of the domain, and hence delays the formation of an ice stream there (Figure 12d). However, the mass source is insufficient to sustain a steady ice stream and is continuously being exhausted, resulting in the ice stream getting narrower. As it narrows, the volume of ice it draws from the other half of the domain $x < 0.5$ diminishes (Figure 12d) and hence the driving stress there can build up to the critical value. Eventually, a stream emerges at $x < 0.5$ and coexists for a while with the initial stream (Figure 13c), but at the same time draws ice away from the initial stream and hasten its stagnation (Figures 13d and 13e). At times, another pattern may occur when the emerging new stream and the initial stream combine into a single, asymmetric wide stream (Figure 13g). This competition over the upstream mass source [e.g., *Anandakrishnan and Alley*, 1997; *Payne and Dongelmans*, 1997; *Payne*, 1999; *Joughin et al.*, 1999] is not present in time-dependent simulations with symmetric initial conditions (compare Figure 12b with Figure 12d).

[38] We find that larger values of the effective viscosity lead to stable, two stream, symmetric solutions. The instability of the symmetric solutions as the shear margin width is increased, in both this section and in section 4.3, is reminiscent of a pitchfork bifurcation which typically occurs in spatially symmetric systems [*Strogatz*, 2001]. However, the unstable symmetric solution as well as the emerging stable asymmetric solutions are all time-dependent here, as opposed to the fixed point (steady state) solutions in the normal form of the pitchfork bifurcation.

5.3. The Role of Ice Rheology Versus Basal Sliding Law

[39] Finally, consider the role of the non-Newtonian rheology versus that of the triple-valued sliding law in causing the observed rich spatiotemporal behavior shown above. We repeated run 1b (Table 2) for several constant (i.e., Newtonian) viscosity values of μ_0, ($1.25\mu_0$, $1.78\mu_0$ and $10\mu_0$), where μ_0 is the minimum effective viscosity from the shear margins of the reference, non-Newtonian simulation (run 1b). The results indicate that, for sufficiently low Newtonian viscosity, the spatial variability patterns in the constant viscosity simulations are essentially the same as in the non-Newtonian case. However, the time scales of the periodicity depend on the effective viscosity used. The three lower-viscosity values listed above resulted in time oscillatory solutions similar to the non-Newtonian run, but with an order of magnitude shorter time scale than the non-Newtonian reference simulation. This period increases with the effective viscosity, but so does the shear margin width. When the Newtonian viscosity is increased in these simulations in an attempt to lengthen the period of the oscillations to its non-Newtonian value, the flow becomes too viscous and the spatiotemporal variability obtains a different character. In the simulation with a constant viscosity of $1.78\mu_0$ the flow was sufficiently viscous that the transverse flushes in the upstream region were eliminated, while the simulation with $10\mu_0$ led to a slow, steady flow with no ice-stream-like patterns. We conclude that the spatial patterns of variability seen, for example, in Figures 5, 7, 8, 12, and 13 are mostly due to the triple-valued sliding law and not the non-Newtonian ice rheology. However, the

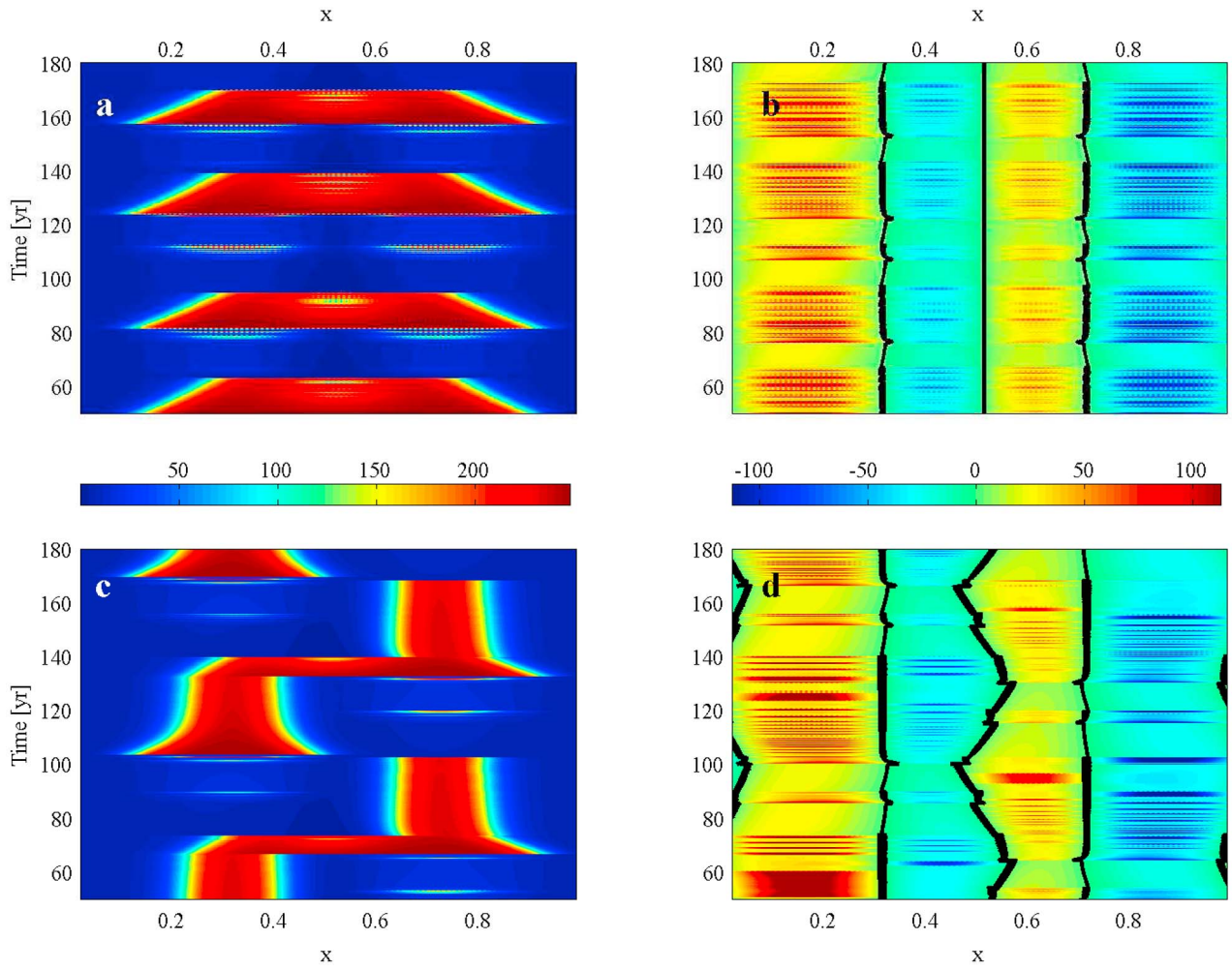

Figure 12. The destabilization of a flow pattern that is symmetric with respect to $x = 0.5$. (a) Values $v(x, t)$ at $y = 0.7$ and (b) $u(x, t)$ at $y = 0.07$, both for a simulation with symmetric initial conditions. (c and d) The same diagnostics and parameters as Figures 12a and 12b but for a simulation with asymmetric initial conditions (color values in meters per year). Figure 12d shows that an active stream on one half of the domain (e.g., $x < 0.5$) drains mass from the upstream part of the other half ($x > 0.5$). Black contours in Figures 12b and 12d mark $u = 0$. Simulation parameters are $M_0 = 15$ m/yr, $n = 3$, $\log_{10} A = -24.7$, $\log_{10} R = -20$, $q_j = 20$, $\sigma_{x_j} = (22, 12, 22)$, $\sigma_y = 10$, $y_0 = 0.3$, $[v] = 125$ m/yr, and $[\tau_b] \simeq 45$ KPa.

shear thinning due to the non-Newtonian rheology allows the model to develop more realistically narrow shear margins and seemingly more relevant temporal variability. Therefore, both the basal sliding law and the non-Newtonian effects play a significant role in the model variability analyzed here.

6. Conclusions

[40] We analyzed ice-stream-like flows due to a triple-valued sliding law and power law ice rheology, using the shelf-stream approximation. The flow was driven by an upstream mass source, specified to be uniform transversely to the ice stream flow. The basal topography was specified to have an upstream ridge with one or two gaps directing the streamflow (Figures 2a and 10a).

[41] The triple-valued sliding law was previously shown to support a bistable flow pattern, where regions of rapid flow coexist with much slower ones [*Fowler and Johnson*, 1996; ST2009]. The present work extends these findings by (1) allowing for a non-Newtonian rheology and (2) investigating the spatiotemporal consequences of the interaction of two adjacent model ice streams.

[42] Considering the flow of a steady ice stream, we first derived and numerically verified a scaling relation between the width of model ice stream shear margins and the ice rheology parameters representing the ice stiffness and the power law exponent. It should be emphasized that we define the shear margin width with relation to the critical velocities, $v_{c\pm}$, in the sliding law (equation (12)), whereas observational data may relate to a different measure related to morphology and surface features. We also showed that the width of the shear margins affects the minimum sustainable width of a

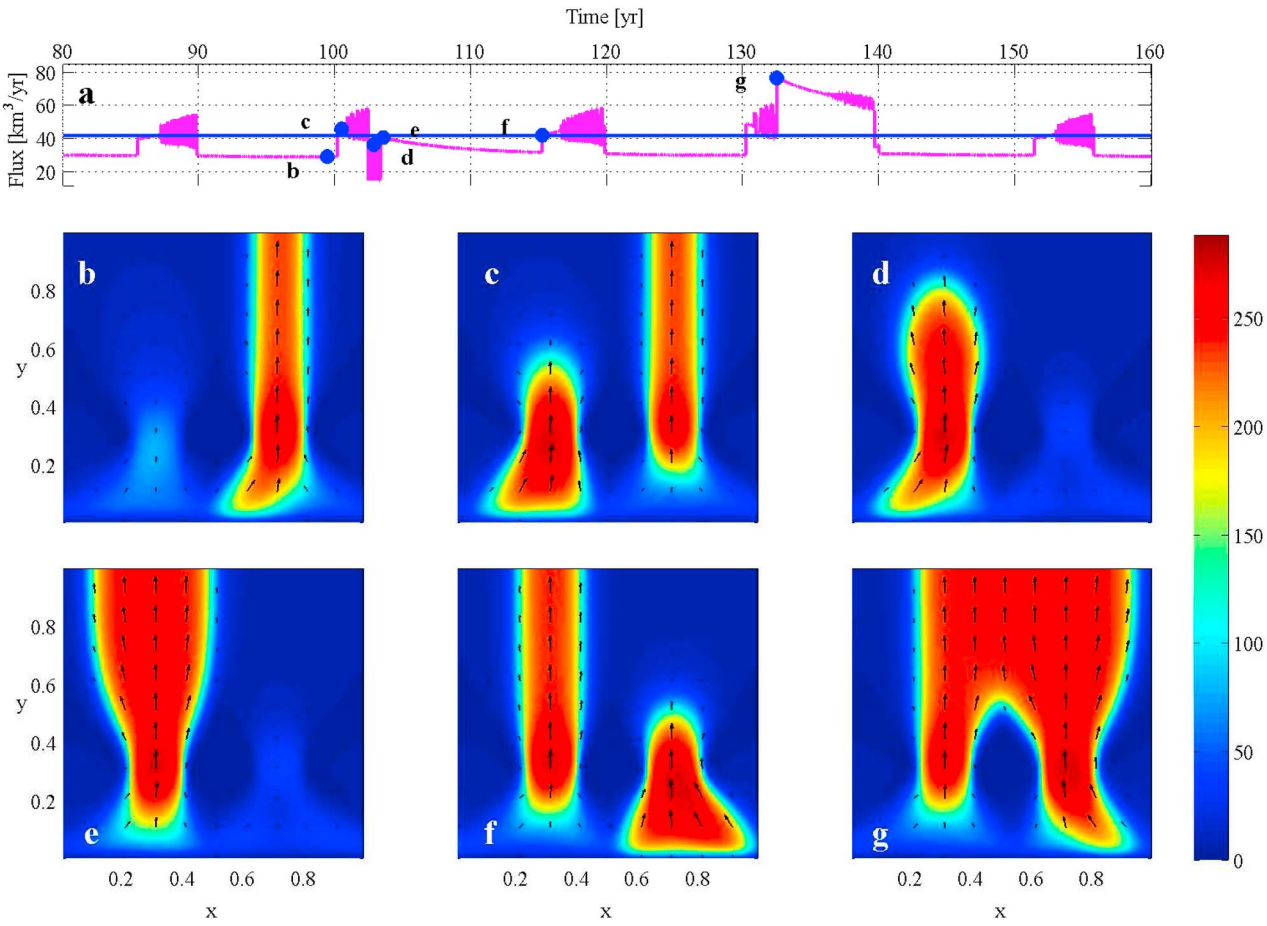

Figure 13. The patterns of flow with asymmetric initial perturbation (simulation parameters identical to those in Figure 12). (a) A time series of the mass flux (cubic kilometers per year) across $y = 0.5$. (b–g) Snapshots of the velocity field (meters per year) corresponding to the filled circles in Figure 13a.

stable model ice stream, as well as the minimum width of an area between two ice streams. The stagnation of an ice stream in our simulations occurs quickly compared with the time the ice streams are active. An ice stream tends to narrow before stagnation and can be tens of kilometers wide immediately before becoming stagnant. These characteristics appear to be roughly consistent with observations (e.g., of Kamb Ice Stream).

[43] Introducing two gaps in the bottom topography led to the formation of two ice streams fed by the same source. We showed that the two streams can remain separated if their shear margins are sufficiently narrow, or may combine into a single wider stream. We explained that the implication is that under a multivalued sliding law there is no intrinsic width to the ice streams, and their maximum width is only limited by the availability of a mass source that can sustain the mass flux carried by a wide stream. Finally, we demonstrated the existence of two-stream solutions that are symmetric with respect to the domain center, have a complex, seemingly aperiodic time behavior, and are unstable. Introducing an asymmetric perturbation to such a symmetric solution resulted in a transition to an asymmetric time-dependent solution where two streams compete over their common source.

[44] Our results indicate that the qualitative spatial patterns of variability we find are a consequence of the triple-valued sliding law. The same patterns are seen with a low constant viscosity (Newtonian rheology), but their time scale is much shorter. Increasing the Newtonian viscosity leads to longer time scales, but the model then loses the ability to simulate the spatiotemporal ice-stream-like variability, and the shear margins become too wide. The non-Newtonian rheology is therefore important for the simulation of spatiotemporal variability at seemingly relevant temporal and spatial scales.

[45] The many two stream solution regimes shown in section 5 display complex time-dependent patterns reminiscent of the spatiotemporal variability of the Siple Coast ice streams. Specifically, we see ice streams that become stagnant at times while others become active, competition for a common mass source, seemingly chaotic behavior in time, shear thinning effects allowing for the existence of narrow shear margins, and merging streams (as observed, for example, by *Joughin et al.* [2002]), all occurring on time scales relevant to those inferred for real ice streams.

[46] The minimal shear margin width in this model is about 5 km, which may be larger than that of some observed margins (*Echelmeyer et al.* [1994] observe a 4–5 km margin).

As emphasized above, we have no pretense of realistically simulating observed ice streams in this work. Instead, we wish to study the effects of the triple-valued sliding law in detail, and this necessarily implies some idealizations. It is still important, of course, that the simulation resolves the *model* shear margins to ensure numerical consistency. Our numerical resolution is sufficient to resolve the shear margin width that is specified through the non-Newtonian ice rheology, and we have confirmed the robustness of some of the key results (e.g., those of Figure 13) by comparison with higher-resolution (1.25 km grid spacing) simulations.

[47] Our model neglects several elements important to the understanding of real ice streams. First, vertical shear is neglected here. This assumption may be valid in regions where bed lubrication is effective and where sliding dominates the velocity field, such as the Siple Coast ice streams; however, vertical shear may become important near ice stream onset areas and between ice streams, which implies that three-dimensional modeling may be necessary to model ice streams properly. The ice stream onset areas are typically steeper, have rougher basal topography, and are probably not as well lubricated as the ice streams. In the presence of vertical deformation, pressure gradients will disperse more efficiently, which may lead to the following outcomes: (1) the basal shear stress may take longer to reach the critical value, making the period in an oscillatory solution longer, and (2) critical basal stress may not be reached at all, preventing flushes in onset regions. Away from the source regions, our model is more likely to be capturing the observed dynamics although one cannot rule out downstream effects due to vertical deformation in the source areas. The interstreams formed in the present model are about 100 times slower than the model ice streams. This implies that the triple-valued sliding law reasonably reproduces interstream ridges although vertical shear is not explicitly included. Nevertheless, it would be interesting to include explicit vertical deformation in order to model the migration time scales of shear margins and the flow in those regions more realistically.

[48] Second, we neglected thermal effects on the viscosity. While the triple-valued sliding law implicitly includes thermal effects at the base of the ice (ST2009), the dependence of ice viscosity on temperature, through the rate factor, A, was neglected. *Jacobson and Raymond* [1998] suggested that such processes may effect the dynamics and stability of the shear margins. Based on our analysis, a temperature-dependent viscosity may result in a distribution of shear margin widths rather than the unique one (calculated here for a given value of A), which may lead to more complex behavior. For example, decreasing the ice temperature from −6°C to −14°C would result in changing $\log_{10} A$ from −24.4 to −24.9, which corresponds to an increase in the shear margin width from ~11 km to ~15 km for $n = 3.15$.

[49] In spite of neglecting these important elements of ice stream dynamics, our simplified description is capable of producing complex spatiotemporal patterns that resemble some of the observed Siple Coast ice stream behaviors. This suggests that it is worthwhile to continue exploring the role of a triple-valued sliding law in ice stream dynamics.

Notation

a Friction law parameter (−0.9).
A Ice stiffness (value varies, see Tables 2 and 3 and Figure 12) ($\mathrm{Pa}^{-n}\ \mathrm{s}^{-1}$).
b Subglacial bed elevation (m).
b_0 Maximum amplitude of bottom topography (1200 m).
g Gravitational acceleration (9.81 m s^{-2}).
h Ice thickness (m).
s Surface elevation (m).
$[L]$ Horizontal length scale (250 km).
$[h]$ Vertical length scales (1800 m).
M Mass source distribution (m s^{-1}).
M_0 Mass source intensity (m s^{-1}).
n Ice flow law exponent (value varies, see Tables 2 and 3 and Figure 12).
$q_1, q_2, q_3, \sigma_{xj}, \sigma_y, x_j, y_0$ Bottom topography parameters (see Table 1).
t Time (s).
$[T]$ Time scale (s).
$\boldsymbol{v} = (u, v), \vartheta$ Velocity field and magnitude (m s^{-1}).
$[v]$ Horizontal velocity scale (value varies, see Tables 2 and 3 and Figure 12) (m s^{-1}).
$v_{c_\pm}$ Friction law critical velocities (m s^{-1}).
x, y Horizontal coordinates (m).
β Sliding law (equation (6)) parameter (50).
μ Ice effective dynamical viscosity (Pa s).
ρ Ice density (900 kg m^{-3}).
σ_m Mass source distribution parameter (0.05 m).
$\boldsymbol{\tau}_b = (\tau_b^x, \tau_b^y)$ Basal shear stresses (Pa).
$[\tau_b]$ Basal shear stress scale (value varies, see Tables 2 and 3 and Figure 12) (Pa).
$\tau_{c_\pm}$ Friction law critical stresses (Pa).
$F_{,x}$ $\partial F/\partial x$.

[50] **Acknowledgments.** We thank Martin Lüthi, three anonymous reviewers, and the associate editor for their detailed and most helpful comments. We thank Jim Rice and Rick O'Connell for helpful discussions and Chris Walker and the FAS computing team for their help with the computational work. This work was supported by the NSF P2C2 program grant 0902844. ET thanks the Weizmann Institute for its hospitality during parts of this work.

References

Anandakrishnan, S., and R. B. Alley (1997), Stagnation of Ice Stream C, West Antarctica by water piracy, *Geophys. Res. Lett.*, *24*, 265–268, doi:10.1029/96GL04016.

Anandakrishnan, S., D. D. Blankenship, R. B. Alley, and P. L. Stoffa (1998), Influence of subglacial geology on the position of a West Antarctic ice stream from seismic observations, *Nature*, *394*(6688), 62–65, doi:10.1038/27889.

Bamber, J., D. Vaughan, and I. Joughin (2000), Widespread complex flow in the interior of the Antarctic ice sheet, *Science*, *287*(5456), 1248–1250, doi:10.1126/science.287.5456.1248.

Barnes, P., D. Tabor, and J. C. F. Walker (1971), Friction and creep of polycrystalline ice, *Proc. R. Soc. London, Ser. A*, *324*(1557), 127–154.

Bell, R. E., D. D. Blankenship, C. A. Finn, D. L. Morse, T. A. Scambos, J. M. Brozena, and S. M. Hodge (1998), Influence of subglacial geology on the onset of a West Antarctic ice stream from aerogeophysical observations, *Nature*, *394*(6688), 58–62, doi:10.1038/27883.

Bennett, M. (2003), Ice streams as the arteries of an ice sheet: their mechanics, stability and significance, *Earth Sci. Rev.*, *61*(3–4), 309–339, doi:10.1016/S0012-8252(02)00130-7.

Bindschadler, R., and P. Vornberger (1998), Changes in the West Antarctic ice sheet since 1963 from declassified satellite photography, *Science*, *279*(5351), 689–692, doi:10.1126/science.279.5351.689.

Catania, G. A., T. A. Scambos, H. Conway, and C. F. Raymond (2006), Sequential stagnation of Kamb Ice Stream, West Antarctica, *Geophys. Res. Lett.*, *33*, L14502, doi:10.1029/2006GL026430.

Conway, H., G. Catania, C. F. Raymond, A. M. Gades, T. A. Scambos, and H. Engelhardt (2002), Switch of flow direction in an Antarctic ice stream, *Nature*, *419*(6906), 465–467, doi:10.1038/nature01081.

Dijkstra, H. A. (2000), *Nonlinear Physical Oceanography*, Kluwer Acad., Dordrecht, Netherlands.

Echelmeyer, K., W. Harrison, C. Larsen, and J. Mitchell (1994), The role of the margins in the dynamics of an active ice stream, *J. Glaciol.*, *40*(136), 527–538.

Fowler, A. C. (1986), A sliding law for glaciers of constant viscosity in the presence of subglacial cavitation, *Proc. R. Soc. London, Ser. A*, *407*(1832), 147–170.

Fowler, A. C. (1987), A theory of glacier surges, *J. Geophys. Res.*, *92*(B9), 9111–9120, doi:10.1029/JB092iB09p09111.

Fowler, A. C., and C. Johnson (1995), Hydraulic run-away: A mechanism for thermally regulated surges of ice sheets, *J. Glaciol.*, *41*(139), 554–561.

Fowler, A. C., and C. Johnson (1996), Ice sheet surging and ice stream formation, *Ann. Glaciol.*, *23*, 68–73.

Fowler, A. C., and E. Schiavi (1998), A theory of ice-sheet surges, *J. Glaciol.*, *44*(146), 104–118.

Gades, A., C. Raymond, H. Conway, and R. Jacobel (2000), Bed properties of Siple Dome and adjacent ice streams, West Antarctica, inferred from radio-echo sounding measurements, *J. Glaciol.*, *46*(152), 88–94, doi:10.3189/172756500781833467.

Goldsby, D. L., and D. L. Kohlstedt (2001), Superplastic deformation of ice: Experimental observations, *J. Geophys. Res.*, *106*, 11,017–11,030, doi:10.1029/2000JB900336.

Greenberg, J. M., and W. Shyong (1990), Surging glacial flows, *IMA J. Appl. Math.*, *45*(3), 195–223, doi:10.1093/imamat/45.3.195.

Heinrich, H. (1988), Origin and consequences of cyclic ice rafting in the Northeast Atlantic Ocean during the past 130,000 years, *Quat. Sci. Rev.*, *29*, 142–152.

Hindmarsh, R. (1998), Ice-stream surface texture, sticky spots, waves and breathers: The coupled flow of ice, till and water, *J. Glaciol.*, *44*(148), 589–614.

Hindmarsh, R. C. A. (2009), Consistent generation of ice-streams via thermo-viscous instabilities modulated by membrane stresses, *Geophys. Res. Lett.*, *36*, L06502, doi:10.1029/2008GL036877.

Hindmarsh, R. C. A., and A. J. Payne (1996), Time-step limits for stable solutions of the ice-sheet equation, *Ann. Glaciol.*, *23*, 74–85.

Hulbe, C. L., and D. R. MacAyeal (1999), A new numerical model of coupled inland ice sheet, ice stream, and ice shelf flow and its application to the West Antarctic Ice Sheet, *J. Geophys. Res.*, *104*(B11), 25,349–25,366, doi:10.1029/1999JB900264.

Hutter, K. (1982a), Dynamics of glaciers and large ice masses, *Annu. Rev. Fluid Mech.*, *14*, 87–130, doi:10.1146/annurev.fl.14.010182.000511.

Hutter, K. (1982b), Glacier flow, *Am. Sci.*, *70*(1), 26–34.

Hutter, K. (1983), *Theoretical Glaciology: Material Science of Ice and the Mechanics of Glaciers and Ice Sheets*, 510 pp., D. Reidel, Dordrecht, Netherlands.

Hutter, K., F. Legerer, and U. Spring (1981), First-order stresses and deformations in glaciers and ice sheets, *J. Glaciol.*, *27*, 227–270.

Jacobel, R. W., T. A. Scambos, N. A. Nereson, and C. F. Raymond (2000), Changes in the margin of Ice Stream C, Antarctica, *J. Glaciol.*, *46*(152), 102–110, doi:10.3189/172756500781833485.

Jacobson, H. P., and C. F. Raymond (1998), Thermal effects on the location of ice stream margins, *J. Geophys. Res.*, *103*(B6), 12,111–12,122, doi:10.1029/98JB00574.

Joughin, I., L. Gray, R. Bindschadler, S. Price, D. Morse, C. Hulbe, K. Mattar, and C. Werner (1999), Tributaries of West Antarctic ice streams revealed by RADARSAT interferometry, *Science*, *286*(5438), 283–286, doi:10.1126/science.286.5438.283.

Joughin, I., S. Tulaczyk, R. Bindschadler, and S. F. Price (2002), Changes in West Antarctic ice stream velocities: Observation and analysis, *J. Geophys. Res.*, *107*(B11), 2289, doi:10.1029/2001JB001029.

Kamb, B. (1987), Glacier surge mechanism based on linked cavity configuration of the basal water conduit system, *J. Geophys. Res.*, *92*(B9), 9083–9100, doi:10.1029/JB092iB09p09083.

Kamb, B. (1991), Rheological nonlinearity and flow instability in the deforming bed mechanism of ice stream motion, *J. Geophys. Res.*, *96*(B10), 16,585–16,595, doi:10.1029/91JB00946.

Kamb, B., C. F. Raymond, W. D. Harrison, H. Engelhardt, K. A. Echelmeyer, N. Humphrey, M. M. Brugman, and T. Pfeffer (1985), Glacier surge mechanism: 1982–1983 surge of Variegated Glacier, Alaska, *Science*, *227*(4686), 469–479, doi:10.1126/science.227.4686.469.

Lliboutry, L. (1969), Contribution á la théorie des ondes glaciaires (in French), *Can. J. Earth Sci.*, *6*(4), 943–953.

MacAyeal, D. R. (1989), Large-scale ice flow over a viscous basal sediment: Theory and application to Ice Stream B, Antarctica, *J. Geophys. Res.*, *94*(B4), 4071–4087, doi:10.1029/JB094iB04p04071.

MacAyeal, D. (1993a), Binge/purge oscillations of the Laurentide Ice Sheet as a cause of the North Atlantic's Heinrich events, *Paleoceanography*, *8*(6), 775–784, doi:10.1029/93PA02200.

MacAyeal, D. (1993b), A low-order model of the Heinrich Event cycle, *Paleoceanography*, *8*(6), 767–773, doi:10.1029/93PA02201.

Marshall, S. J., and G. K. C. Clarke (1997), A continuum mixture model of ice stream thermomechanics in the Laurentide Ice Sheet: 2. Application to the Hudson Strait Ice stream, *J. Geophys. Res.*, *102*(B9), 20,615–20,637, doi:10.1029/97JB01189.

McMeeking, R. M., and R. E. Johnson (1986), On the mechanics of surging glaciers, *J. Glaciol.*, *32*(110), 120–132.

Papanastasiou, T. C., N. Malamataris, and K. Ellwood (1992), A new outflow boundary-condition, *Int. J. Numer. Methods Fluids*, *14*(5), 587–608, doi:10.1002/fld.1650140506.

Pattyn, F. (2003), A new three-dimensional higher-order thermomechanical ice sheet model: Basic sensitivity, ice stream development, and ice flow across subglacial lakes, *J. Geophys. Res.*, *108*(B8), 2382, doi:10.1029/2002JB002329.

Payne, A. J. (1995), Limit cycles in the basal thermal regime of ice sheets, *J. Geophys. Res.*, *100*(B3), 4249–4263, doi:10.1029/94JB02778.

Payne, A. J. (1999), A thermomechanical model of ice flow in West Antarctica, *Clim. Dyn.*, *15*(2), 115–125, doi:10.1007/s003820050271.

Payne, A. J., and P. W. Dongelmans (1997), Self-organization in the thermomechanical flow of ice sheets, *J. Geophys. Res.*, *102*(B6), 12,219–12,233, doi:10.1029/97JB00513.

Payne, A. J., et al. (2000), Results from the EISMINT model intercomparison: the effects of thermomechanical coupling, *J. Glaciol.*, *46*(153), 227–238, doi:10.3189/172756500781832891.

Peters, L. E., S. Anandakrishnan, R. B. Alley, J. P. Winberry, D. E. Voigt, A. M. Smith, and D. L. Morse (2006), Subglacial sediments as a control on the onset and location of two Siple Coast ice streams, West Antarctica, *J. Geophys. Res.*, *111*, B01302, doi:10.1029/2005JB003766.

Raymond, C. F. (2000), Energy balance of ice streams, *J. Glaciol.*, *46*(155), 665–674, doi:10.3189/172756500781832701.

Raymond, C. F., K. A. Echelmeyer, I. M. Whillans, and C. S. M. Doake (2001), Ice stream shear margins, in *The West Antarctic Ice Sheet: Behavior and Environment*, *Antarct. Res. Ser.*, vol. 77, edited by R. B. Alley and R. A. Bindschadler, pp. 137–155, AGU, Washington, D. C.

Retzlaff, R., and C. R. Bentley (1993), Timing of stagnation of Ice Stream C, West Antarctica, from short-pulse radar studies of buried surface crevasses, *J. Glaciol.*, *39*(133), 553–561.

Saito, F., A. Abe-Ouchi, and H. Blatter (2006), European Ice Sheet Modelling Initiative (EISMINT) model intercomparison experiments with first-order mechanics, *J. Geophys. Res.*, *111*, F02012, doi:10.1029/2004JF000273.

Sayag, R. (2009), Dynamics and spatiotemporal variability of ice streams, Ph.D. thesis, Harvard Univ., Cambridge, Mass.

Sayag, R., and E. Tziperman (2008), Spontaneous generation of pure ice streams via flow instability: Role of longitudinal shear stresses and subglacial till, *J. Geophys. Res.*, *113*, B05411, doi:10.1029/2007JB005228.

Sayag, R., and E. Tziperman (2009), Spatiotemporal dynamics of ice streams due to a triple-valued sliding law, *J. Fluid Mech.*, *640*, 483–505, doi:10.1017/S0022112009991406.

Schoof, C. (2004a), Bed topography and surges in ice streams, *Geophys. Res. Lett.*, *31*, L06401, doi:10.1029/2003GL018807.

Schoof, C. (2004b), On the mechanics of ice-stream shear margins, *J. Glaciol.*, *50*(169), 208–218, doi:10.3189/172756504781830024.

Schoof, C. (2006), A variational approach to ice stream flow, *J. Fluid Mech.*, *556*, 227–251, doi:10.1017/S0022112006009591.

Stokes, C. R., C. D. Clark, O. B. Lian, and S. Tulaczyk (2007), Ice stream sticky spots: A review of their identification and influence beneath contemporary and palaeo-ice streams, *Earth Sci. Rev.*, *81*(3–4), 217–249, doi:10.1016/j.earscirev.2007.01.002.

Strogatz, S. H. (2001), *Nonlinear Dynamics and Chaos: With Applications to Physics, Biology, Chemistry and Engineering*, 498 pp., Westview, Boulder, Colo.

Truffer, M., and K. A. Echelmeyer (2003), Of isbræand ice streams, *Ann. Glaciol.*, *36*, 66–72, doi:10.3189/172756403781816347.

Tulaczyk, S., W. Kamb, and H. Engelhardt (2000), Basal mechanics of Ice Stream B, West Antarctica: 2. Undrained plastic bed model, *J. Geophys. Res.*, *105*(B1), 483–494, doi:10.1029/1999JB900328.

Walder, J. S. (1982), Stability of sheet flow of water beneath temperate glaciers and implications for glacier surging, *J. Glaciol.*, *28*(99), 273–293.

Weertman, J. (1964), The theory of glacier sliding, *J. Glaciol.*, *5*(39), 287–303.

R. Sayag, Department of Applied Mathematics and Theoretical Physics, University of Cambridge, Wilberforce Road, Cambridge CB3 0WA, UK. (r.sayag@damtp.cam.ac.uk)

E. Tziperman, Department of Earth and Planetary Science, Harvard University, 20 Oxford St., Cambridge, MA 02138, USA. (eli@eps.harvard.edu)